HIGH-RESOLUTION RAINFALL RATE AND DSD ESTIMATION FROM X-BAND POLARIMETRIC RADAR MEASUREMENTS

Marios N. Anagnostou[1], *Emmanouil N. Anagnostou*[2], and Witold F. Krajewski[3]
[1,2]Department of Civil and Environmental Engineering,
University of Connecticut, Storrs, CT

[3]IIHR-Hydroscience and Engineering
The University of Iowa, Iowa City, IA

Email: [1]ma111@engr.uconn.edu, [2]manos@engr.uconn.edu, [3] witold-krajewski@uiowa.edu;

Abstract

This study proposes investigation of new attenuation correction and microphysical retrieval methods for X-band polarimetric radar (XPOL). It will concentrate on exploring the dependence of the retrieval on raindrop size distribution variability, and its sensitivity with respect to the selection of oblateness-size relation (or axial ratio) and maximum diameter limit. Variations in the assumed form of the raindrop axial ratio may result in significant biases in attenuation and microphysical retrievals. In addition, at this wavelength, resonance occurs for sizes larger than about 4 mm, and therefore several polarimetric variables exhibit non-monotone dependence on the drop diameter. An algorithm is developed and experimentally validated for retrieving DSD model parameters. The DSD model is assumed to be a three-parameter "normalized" gamma distribution. Coincidental and closely matched radar rays from non-attenuated (S-band) dual-polarization radar measurements and corresponding DSD retrievals are used to validate the proposed XPOL algorithm in terms of attenuation correction, as well as DSD parameter retrievals.

Key Words: polarimetric radar, drop size distribution, precipitation, estimation.

1. Introduction

From the first stages of dual-polarization weather radar development, 10-cm wavelength and a linear polarization basis (horizontal *H* and vertical *V*) became a favourite choice by a majority of investigators (Zirnic 1996). The physical concept behind polarization diversity is that falling raindrops take oblate shape, which under equilibrium condition can be related to their volume (Pruppacher and Beard 1970). This non-spherical raindrop geometry impacts both propagation and backscatter of an incoming *H* and *V* polarization electromagnetic radar wave. The most common polarimetric radar measurements used in rainfall estimation are the reflectivity factors at *H* and *V* polarization (Z_H, Z_V, in mm^6/m^3); the differential reflectivity factor (Z_{DR}, dimensionless), which is defined as the ratio of Z_H to Z_V; and the propagation differential phase shift (Φ_{DP}, in degrees), which is the difference in the two-way phase change between horizontally and vertically polarized waves increased with distance through rain. Over a certain radial distance (Δr) one can calculate the specific differential phase shift (K_{DP}, in degrees/km) as one-half of Φ_{DP} gradient.

The main goal of polarization diversity has always been the improvement of radar rainfall estimation. Seliga and Bringi (1976) were among the first to suggest the use of polarimetric measurements for the retrieval of raindrop size distribution and mainly focused on the estimation of D_0 (the median volume diameter) or D_m (the mass-weighted mean diameter) using only Z_{DR}

measurements. Many rainfall estimation techniques have been developed since the early study of Seliga and Bringi (1976), but primarily for radar frequencies that are not significantly affected by hydrometeor attenuation and non-Rayleigh scattering effects (Goddard and Cherry 1984; Aydin et al. 1987; Bringi et al. 1998; Bringi et al. 2002). Such radar frequencies (i.e., *S*-band) are basically used for operational radar systems like the WSR-88D network in the United States and for experimental units used in the measurement of high rain rates and mixed phase precipitation.

On the other hand, *X*-band systems have not been extensively used for microphysical retrievals and quantitative precipitation estimation due to the increased sensitivity of shorter wavelengths on attenuation and resonance effects, which can be severe in high concentrations of large raindrops. Nevertheless, the *X*-band frequency can be advantageous over longer wavelengths (*C*- and *S*-band) in measuring light to moderate rainfall (Anagnostou et al. 2003, Matrosov et al. 1999, 2002). At long wavelengths such as ~10 cm, the propagation differential phase shift has low sensitivity to rainfall rate, thus, estimation of rainfall rate requires significant integration along-a-ray. In the Rayleigh scattering regime, the magnitude of K_{DP} is proportional to the reciprocal of the radar wavelength. Therefore shorter wavelengths are associated with greater phase change per unit rainfall rate (e.g., *X*-band sensitivity is about three times the one of *S*-band). For example, Blackman and Illingworth (1997) have shown that to retrieve a rainfall rate of 8 mm/h from K_{DP} at *S*-band would require Δr of at least 5 km at 25 km radar range.

However, an important issue to be taken into consideration are the random fluctuations in Φ_{DP} and the differential phase shift on backscatter; a resonance effect that is part of the total differential phase shift (also known as "δ" effect) that cannot be readily separated from Φ_{DP} data (e.g., Matrosov et al. 2002; Keenan et al. 2001; Zirnic and Ryzhkov 1996; Hubbert and Bringi 1995). The δ value can be significant at short radar wavelengths, especially when sufficient concentration of large (> 6 mm at *C*-band and > 3.5 mm at *X*-band) raindrops is encountered in the radar sampling volume, which is more common in high rainfall intensities (Zrnic et al. 2000). This non-Rayleigh effect may introduce complications at *C*- and *X*-band frequencies, and requires careful consideration when K_{DP} is used in quantitative applications such as for attenuation correction of reflectivity and differential reflectivity measurements (Anagnostou et al. 2003; Matrosov et al. 2002; Keenan et al. 2001).

Once, the major limitation of *X*-band has been addressed correctly, the use of this wavelength would allow more accurate microphysical retrievals and rainfall estimation for low or moderate rainfall rates from the current *C*- and *S*-band systems. In addition, it provides higher resolution; better sensitivity on detecting weak targets and it is less susceptible to anomalous propagation effect. Such systems could possibly be used to fill up critical gaps on the coverage of large operational radar networks.

In this study we will discuss the issue of attenuation correction and DSD estimation at *X*-band. The *XPOL* algorithm procedures for attenuation correction and DSD parameter estimation will be validated and assessed using coincidental non-attenuated (*S*-band) radar measurements and corresponding DSD retrievals.

2. Experimental Data

To facilitate this research we compare several storm cases measured coincidentally by two weather research radars deployed in the International H_20 Project (*IHOP*). The first is an *X*-band dual-polarization Doppler radar on wheals (*XPOL*) and the second is *NCAR*'s *S*-band (*SPOL*) polarimetric radar. *XPOL*'s field deployment in *IHOP* supported a number of objectives including convective initiation, atmospheric boundary layer, and our own research on quantitative precipitation estimation. During *MCS* (Mesoscale Convective Systems) developments in the vicinity of *SPOL* (situated at a farm approximately 30 miles south of Liberal, KN), *XPOL* was deployed a few meters ahead of *SPOL* and the two radars were operated at closely matched scanning strategies. During a storm development multiple elevation *PPI* (Plan Position Indicator) sector

scans and *RHI* (Range Height Indicator) scans at selected azimuths were selected. *IHOP* experiment lasted about two months, from May 16 to July 22 of 2002, during which several storm cases of varying intensity and structure were observed. Table 1 summarizes the storm events measured coincidentally by the two radars.

3. Background

In this section we summarize the basic physical relationships between integrated radar and rainfall parameters and DSD. The radar parameters considered here are the *X*-band measured (attenuated) reflectivity at both polarizations *H* and *V*, Z_{aH} and Z_{aV} (in mm^6m^{-3}) from this we derive the attenuated differential reflectivity, $Z_{aDR} = Z_{aH}/Z_{aV}$ (in decibels, dB) the differential phase shift, which is the phase shift of both the forward and backscatter phase shift between *H* and *V* polarizations, Φ_{DP} (in degrees) from this we derive the specific differential phase shift by taking its gradient along a radar ray, K_{DP} (degrees/km). All these measurements can be related to equivalent (non-attenuated) radar parameters as follows:

$$Z_{aH}(r) = Z_{eH}(r) \times 10^{-0.2\int_0^r A_H(s)ds}$$
$$Z_{aV}(r) = Z_{eV}(r) \times 10^{-0.2\int_0^r A_V(s)ds} \quad (1)$$

$$Z_{\mathrm{aDR}}(\mathrm{r}) = Z_{\mathrm{DR}}(\mathrm{r}) \times 10^{-0.2\int_0^{\mathrm{r}} A_{\mathrm{DP}}(\mathrm{s})\mathrm{ds}} \quad (2)$$

$$\Phi_{\mathrm{DP}}(\mathrm{r}) = \delta(\mathrm{r}) + 2\int_0^{\mathrm{r}} K_{\mathrm{DP}}(\mathrm{s})\mathrm{ds} \quad (3)$$

where Z_{eH}, Z_{eV} and Z_{DR} are the *H* and *V* equivalent (non-attenuated) radar reflectivity and differential reflectivity parameters, A_H, A_V, and A_{DP} (dB/km) are the *H* and *V* specific attenuation and differential attenuation parameters, respectively, and K_{DP} is the specific differential phase shift (degrees/km), which is the gradient of Φ_{DP} along a ray. These parameters are related to the hydrometeor size distribution (DSD) within a radar sampling volume through the following integral equations (Bringi and Chandrasekar 2002):

$$Z_{eH,V} = \frac{\lambda^4}{\pi^5}\left|\frac{m^2+2}{m^2-1}\right|^2 \int_0^{D_{\max}} \sigma_{bH,V}(D_e)\cdot N(D_e)\cdot dD_e \quad (4)$$

$$A_{H,V} = 2\lambda \int_0^{D_{\max}} \mathrm{Im}\left[f_{H,V}(K_1, K_1; D_e)\right]\cdot N(D_e)\cdot dD_e \quad (5)$$

$$K_{DP} = \lambda \int \left(\mathrm{Re}\left[f_H(K_1, K_1; D_e)\right] - \mathrm{Re}\left[f_V(K_1, K_1; D_e)\right]\right)\cdot N(D_e)\cdot dD_e \quad (6)$$

$$\delta = \arg\left[\int_0^{D_{\max}} f_H(K_1, -K_1; D_e)\cdot f_V^{\,*}(K_1, -K_1; D_e)\cdot N(D_e)\cdot dD_e\right] \quad (7)$$

where D_e is the equivolumetric spherical diameter, $N(D_e)$ the number of drops in $[D_e, D_e+dD_e]$ range, λ is the radar wavelength, m the complex refractive index of the hydrometeors, and δ the backscattering phase shift. The *H* and *V* polarization backscattering cross sections, $\sigma_{bH,V}(D_e)$, and the forward, $f_{H,V}(K_1,K_1;D_e)$, and backward, $f_{H,V}(K_1,-K_1;D_e)$, scattering coefficients can be calculated for an assumed DSD parameterization and raindrop oblateness-size relation using the *T-matrix* method (Barber and Yeh 1975). In the following we discuss aspects of DSD modeling and drop oblateness-size relations derived on the basis of observed DSD spectra.

3.1. *Raindrop size distribution model*

The polarimetric radar measurements are related to the RSD as discussed above. Ulbrigh (1983) assumed a normalized Gamma distribution model for representing raindrop spectrum as

$$N(D) = N_W f(\mu)\left(\frac{D}{D_0}\right)^{\mu} e^{-(4+\mu)\left(\frac{D}{D_0}\right)} \qquad (\text{m}^{-3}\text{mm}^{-1}) \tag{8}$$

with

$$f(\mu) = \frac{6}{4^4}\frac{(4+\mu)^{(\mu+4)}}{\Gamma(\mu+4)} \tag{9}$$

where N_w is the normalized intercept parameter of an equivalent exponential DSD that has the same water content and median volume diameter (D_0) as the gamma DSD. The normalized gamma DSD parameter values are derived on the basis of 3-min-averaged DSD spectra; where the three parameters (N_w, D_0, μ) are obtained as following. The water content (W, in gm^{-3}) and the mass-weighted mean diameter (D_m, in mm) are calculated first, based on which we obtain N_w as,

$$N_w = \left(\frac{256}{\pi}\right)\left(\frac{1000W}{D_m^4}\right) \quad (\text{m}^{-3}\text{mm}^{-1}) \tag{10}$$

The normalized DSD is then constructed as $N(x) = N(D/D_m)/N_w$, and μ is estimated by minimizing the least square deviation between log [$N(x)$] and $log\ \{f(\mu)x^{\mu}exp\ [-(4+\mu)x]\}$ where $x = D/D_m$.

For each 3-min-averaged gamma DSD parameters, we run the *T-matrix* scattering calculation algorithm to compute the simulated radar measurements (Z_h, Z_{dr}, and K_{dp}) at 9.3 GHz for *X*-band and 2.8 GHz for *S*-band, assuming that the mean axis ratio fit used in these simulations is the one recommended by Andsager et al. (1999) for $1 \le D \le 4$ mm, and the Beard and Chuang (1987) equilibrium axis ration fit for $D<1$ and $D>4$ mm; Gaussian canting angle distribution with mean 0° and standard deviation of 10°; and size integration up to 6 mm.

4. Methodology

Meteorological radars that require relatively high spatial resolution are limited on the required size of the antenna and the transmitted power, however, they desire the use of higher frequencies and even though these systems are small and versatile their signal might undergo significant attenuation by the medium as it travels to and from the rain scattering volume of interest. Here we suggested the use of an existing attenuation correction algorithm that goes back to the work of Hitschfeld and Bordan (Hitschfeld and Bordan 1954) that has been extensively used for the attenuation correction of airborne or spaceborne radar (Meneghini 1978; Iguchi and Meneghini 1994) and ground radar (Anagnostou et al. 2003).

4.1. *XPOL* Attenuation Correction Algorithm

The algorithm proposed here corrects for the horizontal and differential reflectivity (Z_h and Z_{dr}) attenuation by evaluating the integral equations (1) and (2) along a radar ray. The specific attenuation and differential attenuation are related quasi-linearly with the specific differential phase shift and specific attenuation, respectively. Thus, we use estimates of the specific and differential attenuation cumulations along a ray path derived from Ψ_{dp} (here we use $\Psi_{dp} = \Phi_{dp} + \delta$, where δ is the backscattering phase shift) profile as following:

$$\int_0^r A_H(r)dr = \gamma(\beta) \times \left[\Psi_{DP}(r) - \Psi_{DP}(0)\right], \tag{11}$$

and

$$\int_0^r A_{DP}(r)dr = \varphi(\beta) \times \int_0^r A_H(r)dr \,. \tag{12}$$

where γ and f are coefficient derived from the scattering calculation and are related to the β_d slope of the shape-size relation $\left(d(\alpha/\beta)/dD \right)$ where the α/β is the axis ratio. Of course, in this study we use one axial ratio, but it is still under investigation as to which optimal axial ratio model should we use. Then we substitute the estimated specific and differential attenuation estimates to (1) and (2) to derive the equivalent horizontal and differential reflectivity.

4.2. The XPOL DSD Retrieval

Having corrected XPOL measurements for attenuation, we proceed with the estimation of the DSD parameters (N_w, D_0 and μ). The *XPOL* DSD algorithm is based on experimental relationships derived from *T-matrix* scattering simulations. The algorithm is based on the following two parameterizations in the sequence order presented below:

$$\begin{aligned} \mu &= f(Z_{dr}), \\ N_w &= f(Z_h, \mu), \end{aligned} \tag{15}$$

The functions are in the form of look up tables derived from scattering calculations using DSD spectra. The third parameter, the median drop diameter (D_0) is estimated using the following relation

$$D_0 = \frac{3.67 + \mu}{\Lambda}, \tag{16}$$

whereas the Λ is calculated using the μ-Λ constrain relationship derived from measured raindrop spectra.

5. Discussion

As an example Figure 1 illustrates the *XPOL*'s attenuation correction. For this case we take one match-ray profile from both *XPOL* and *SPOL* radar from June 16th on the same azimuth and elevation with 10 sec time difference.

At the first panel of the Figure we compare the horizontal reflectivity, at the second the differential reflectivity, and at the bottom panel the differential phase shift. At the first two panels, the blue line is the *XPOL*'s raw data, while the black line is the *SPOL*'s raw data. The red line presents the attenuation correction for both XPOL horizontal and differential reflectivity. At the last panel, the blue line presents the *XPOL*'s differential phase shift, while the *black line represents the SPOL's phase shift*. The red line is the filtered data applied to the *XPOL*'s differential phase shift raw data. The significant issue that should be noted here is the sensitivity of *X*-band's differential phase shift compared to the *S*-band. We see that the X-band Φ_{DP} ray profile is about three times more sensitive to the change of rainfall compared to the corresponding S-band Φ_{DP} profile.

In Figure 2 we compare from the same ray, the three DSD parameters derived from *XPOL* and *SPOL* measurements. For the SPOL DSD retrieval we used Bringi et al. (2002) method. In the first panel we compare the intercepted parameter ($log_{10}(N_w)$). The blue line represents the *XPOL* retrieval, while the black line the corresponding *SPOL* retrieval. The same applies for the other two panels. We note that there is a good agreement between the XPOL and SPOL DSD estimates, which indicates a consistent performance for the XPOL algorithm.

On the next figure (Figure 3) we illustrate the horizontal and differential reflectivity ray profiles. These profiles are calculated from the scattering simulations, using the DSD parameters estimated from the Bringi's et al. 2002 method and the *XPOL* DSD algorithm. We can note again a good agreement in both profiles, even though there is some low bias in reflectivity values below 30 dBZ (first panel). In differential reflectivity, even though there is some small bias at the pick values of the ray (at about 12.5 Km range there is a bias of ~ 0.6 dB) there is an overall good agreement between the two simulated profiles. The agreement is also good between the simulated and measured SPOL profiles.

6. Conclusions

An *X*-band Polarimetric and Doppler radar on wheals (*XPOL*) was deployed in Liberal, KS as part of the *IHOP* field campaign. The *XPOL*'s primary objectives were to provide quantitative rainfall and microphysical measurements taking coincidental measurements with *SPOL*. Combining those measurements from both radars we aim at assessing our existing *XPOL* attenuation correction algorithm by comparing matched *X*-band and *S*-band rays and DSD parameter retrievals.

The development of the algorithm involved specific and differential attenuation correction ray profiles measured by *XPOL*, filtering the Φ_{dp} profile to remove noise and potential folding and δ effect, and the retrieval of the three parameters of an assumed "normalized" Gamma DSD model.

To assess the *XPOL* algorithm and DSD retrievals, as an example we took one of the many cases, on June 16th where we match both *XPOL*'s and *SPOL*'s ray profiles. We apply the *XPOL* algorithm for this case and we correct for the horizontal and differential reflectivity. We compare the corrected results with *SPOL*'s horizontal and differential reflectivity.

For the same case, we assessed *XPOL*'s DSD algorithm. First, we retrieved the *SPOL*'s DSD parameters using an existing algorithm, suggested by Bringi et al. (2002), and then we compared these results with those derived from our *XPOL* retrieval. The agreement was very good in terms of both DSD parameters and simulated radar parameters.

Further investigations will concentrate on studying different axial ratio models and maximum diameter (D_{max}) integration and selecting the optimum model and D_{max}. By combining two different wavelengths will help on the better understudying of the mixed phase microphysics and improve its retrieval from ground radar.

7. Acknowledgements

The study was supported by NSF CAREER Grant EAR0132942 to Prof. Emmanouil Anagnostou at the University of Connecticut.

8. References

Anagnostou E.N., Anagnostou M.N., Witold F. Krajewski, Anton Kruger, and Benjamin J. Miriovsky, High-Resolution Rainfall Estimation from X-Band Polarimetric Radar Measurements, (submitted to Journal of Hydrometeorology 2003).

Aydin, K., H. Direskeneli, and T.A.Seliga, Dual-polarization radar estimation of rainfall parameters compared with ground-based disdrometer measurements. October 29, 1982, central Illinois experiment, *IEEE Trans. Geosci. Remote Sens.,* GE-25, 834-844, 1987.

Barber, P and C. Yeh, Scattering of electromagnetic waves by arbitrarily shaped dielectric bodies, *Applied Opt.,* 14*,* 2864-2872, 1975.

Beard, K.V., and C. Chuang, A new model for the equilibrium shape of raindrops, *J. Atmos. Sci.*, 44, 1509-1524, 1987.

Blackman, T.M., and A.J. Illingworth, Examining the lower limit of KDP rain-rate estimation including a case study at S-band, Preprints, *28th Inter. Conf. On Radar Meteor*., Austin, TX, Amer. Meteor. Soc., 117-118, 1997.

Bringi, V.N., and V. Chandrasekar, *Polarimetric Doppler Weather Radar: Principles and Applications*, Cambridge University Press, 2002.

Bringi, V.N., Huang, Gwo-Jong, V. Chandrasekar, Gorgucci E., A methodology for estimating the parameters of gamma raindrop size distribution model from polarimetric radar data: Application to a squall-line event from the TRMM/Brazil Campaign, *of Atmospheric and Oceanic Technology*, 19(5), 633–645, 2002.

Bringi, V.N., V. Chandrasekar, and R. Xiao, Raindrop axis ratios and size distributions in Florida rainshafts: An assessment of multiparameter radar algorithms, *IEEE Trans. Geosci. Remote Sens.*, 36, 703-715, 1998.

Goddard, J.W.F., and S.M.Cherry, The ability of dual-polarization radar (copular linear) to predict rainfall rate and microwave attenuation, *radio Sci., 19, 201-208, 1984.*

Hitschfeld, W., and J. Bordan, Errors inherent in the radar measurement of rainfall at attenuating wavelengths, *J. Meteor.*, 11, 58-67, 1954.

Hubbert, J.V., and V.N. Bringi, An iterative filtering technique for the analysis of coplanar differential phase and dual-frequency radar measurements. *J. Atmos. Oceanic Technol*., 12, 643-648, 1995.

Iguchi, T., and Meneghini, R., Intercomparison of single-frequency methods for retriving a vertical rain profile from airborne or spaceborne radar data, *J. Atmos. Oceanic Technol*., 11, 1507-1516, 1994.

Keenan, T. D., Carey, L. D., Zrnić, D. S., May, P. T., Sensitivity of 5-cm Wavelength Polarimetric Radar Variables to Raindrop Axial Ratio and Drop Size Distribution, *J. Appl. Meteor.*, 40(3), 526–545, 2001.

Matrosov, S.Y., K.A. Clark, B.E. Martner, A. Tokay, X-band polarimetric radar measurements of rainfall, *J. Appl. Meteor*., 41, 941-952, 2002.

Matrosov, S.Y., R.A. Kropfli, R.F. Reinking, and B.E. Martner, Prospects for measuring rainfall using propagation differential phase in X- and Ka-radar bands, *J. Appl. Meteor*., 38, 766-776, 1999.

Meneghini, R., Rain-rate estimates for an attenuating radar, *Radio Sci.,* 13, 459-470, 1978.

Pruppacher H.R., and K.V. Beard, A wind tunnel investigation of the internal circulation and shape of water drops falling at terminal velocity in air, *Quart. J. Roy. Meteor. Soc*., 96, 247-256, 1970.

Seliga, T. A., V. N. Bringi, Potential Use of Radar Differential Reflectivity Measurements at Orthogonal Polarizations for Measuring Precipitation, *J. Appl. Meteor.,* 15, 69-75, 1976.

Ulbrigh, C.W., Natural variation in the analytical form of the raindrop size distribution, *J. Appl. Meteor*, 22, 1764-1775, 1983.

Zrnić D. S., and A.V. Ryzhkov, Advantages of rain measurements using specific differential phase, *J. Atmos. Oceanic Technol*., 13, 454-464, 1996.

Zrnić D. S., T. D. Keenan, L. D. Carey, and P. May, Sensitivity analysis of polarimetric variables at a 5-cm wavelength in rain, *J. Appl. Meteor.,* 39, 1514-1526, 2000.

9. Tables

Table 1 Date/time and duration of storm cases observed jointly by XPOL and SPOL during the IHOP 2002 experiment.

Storm Period (Date and time in UTC)	*Duration* (hr:mm)
May 17, 00:23 – May 17, 03:00	02:37
May 26,18:53 – May 26, 19:05	00:12
May 27, 15:56 – May 27, 16:13	00:17
June 04, 19:08 – June 04, 21:08	02:00
June 15, 23:20 – June 16, 01:20	02:00

10. Figures

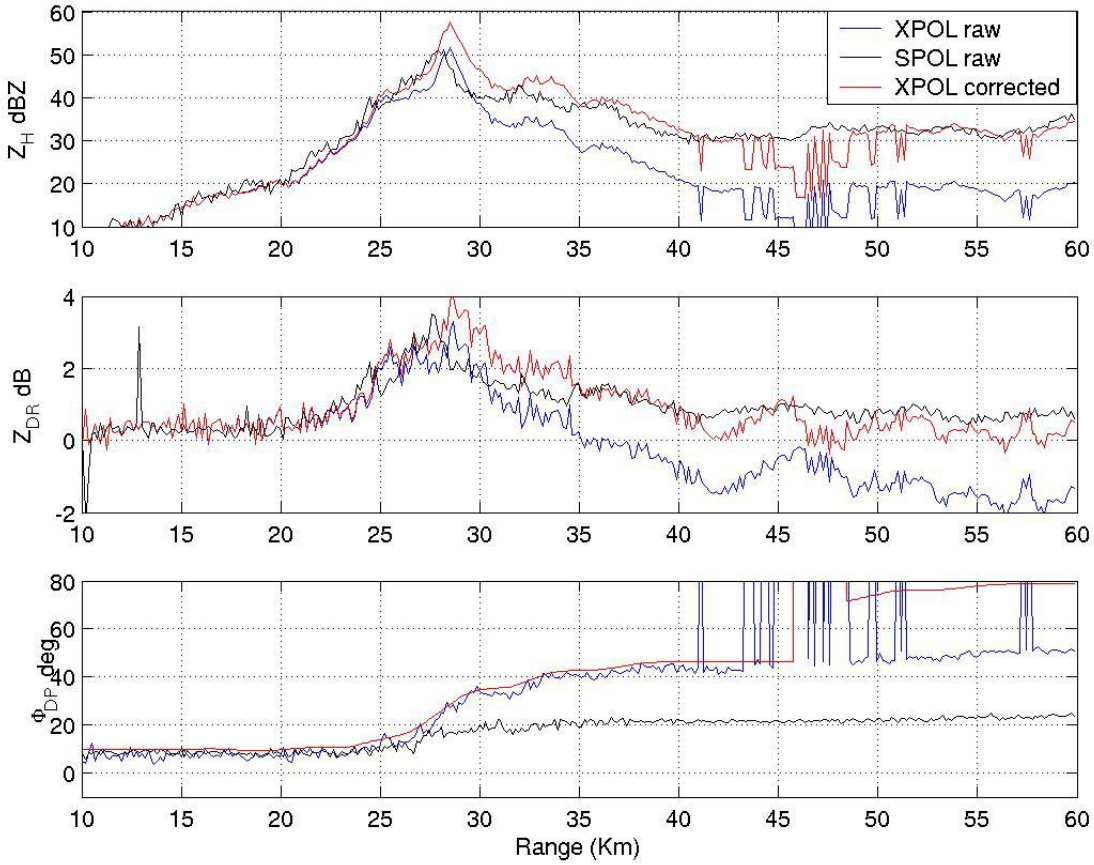

Fig. 1 A sample ray plot from June 16, 2002 case study.

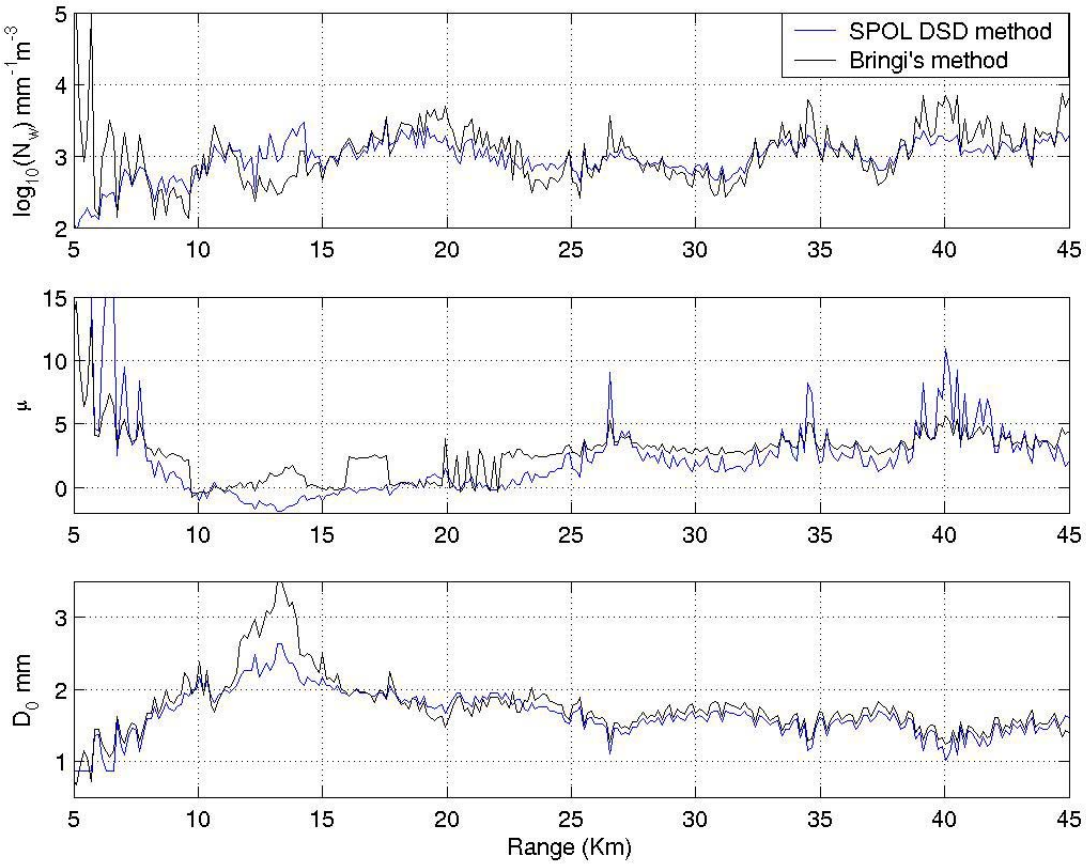

Fig. 2 Comparison between SPOL and XPOL DSD retrievals for the ray shown in Figure 1.

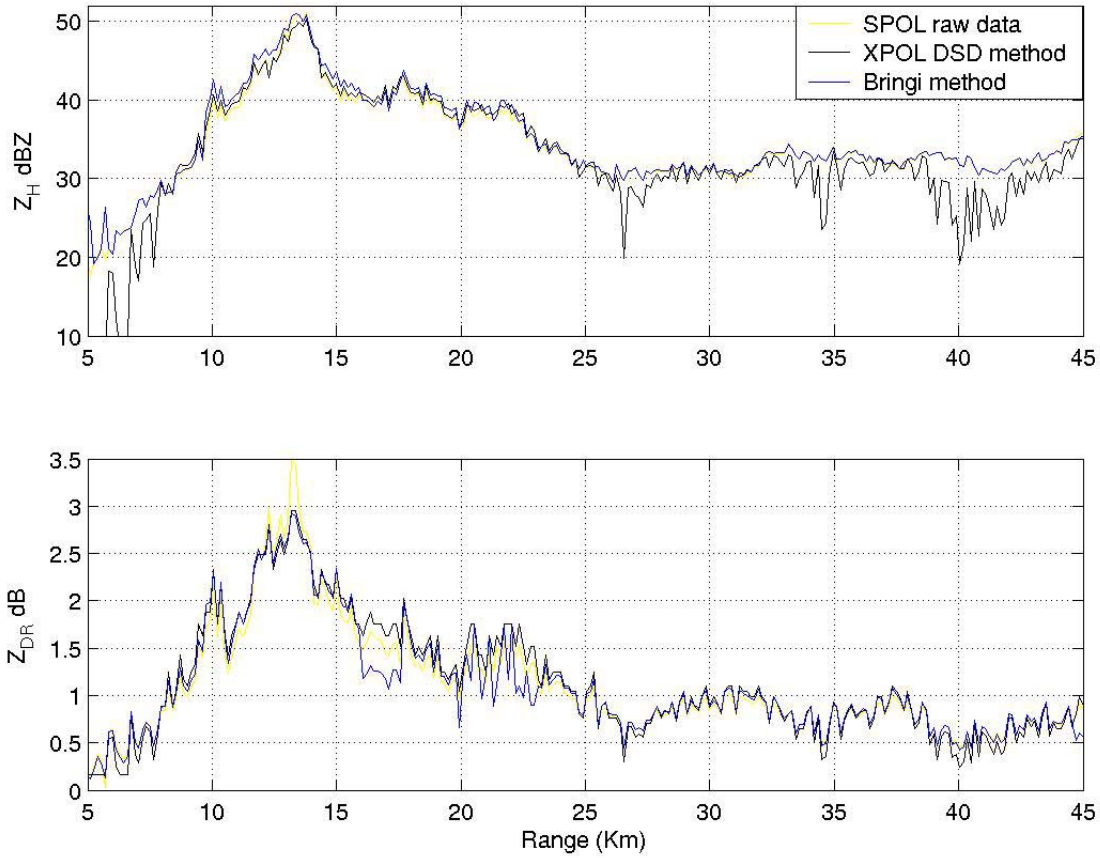

Fig. 3 **Comparison of S-band simulated reflectivity and differential reflectivity ray plots derived on the basis of retrieved XPOL and SPOL DSD parameters. The raw SPOL measurements are overlayed for comparison.**